NACA RM A9F16



NACA

# RESEARCH MEMORANDUM

## A COMPARISON OF TWO SUBMERGED INLETS AT SUBSONIC AND TRANSONIC SPEEDS

By Emmet A. Mossman

Ames Aeronautical Laboratory
Moffett Field, Calif.



NATIONAL ADVISORY COMMITTEE
FOR AERONAUTICS

WASHINGTON
September 15, 1949

NATIONAL ADVISORY COMMITTEE FOR AERONAUTICS

RESEARCH MEMORANDUM

# A COMPARISON OF TWO SUBMERGED INLETS AT SUBSONIC AND TRANSONIC SPEEDS

By Emmet A. Mossman

## SUMMARY

Operation of two submerged-type inlets has been simulated in a 2.1- by 7.4-inch wind tunnel at subsonic and transonic speeds. One inlet corresponded to a parallel-walled submerged intake, and the other to an NACA submerged inlet, a type which has divergent ramp walls. A qualitative comparison of the inlets is made on the basis of pressure recovery. Shadowgraphs of the air flow are also presented.

The pressure recovery was relatively constant throughout the lower subsonic speed range. However, a sharp decrease in pressure recovery with the parallel-walled inlet occurred simultaneously with the appearance of weak shock-wave disturbances at the start of the ramp. This decrease in pressure recovery occurred at free-stream Mach numbers between 0.75 and 0.82, depending on the mass-flow ratio. With the divergent-walled inlet the corresponding Mach number range was 0.90 to 0.94, although shock waves formed along the ramp at a lower free-stream Mach number.

The ability of the divergent-walled inlet to operate with satisfactory pressure recovery at higher free-stream Mach numbers than was possible with the parallel-walled inlet is attributed to the difference in the boundary-layer characteristics of the two types of inlets.

## INTRODUCTION

Because many present-day airplanes are designed to fly in or through the high subsonic and transonic speed range, the need for data on air inlets at these velocities has become increasingly urgent. Although some data are available on nose inlets, little research has been done on submerged inlets in the transonic speed range. Data obtained up to a Mach number of 0.875 on an NACA submerged inlet have shown that satisfactory air-induction characteristics could be attained at subsonic speeds. (See references 1, 2, and 3.)

This report covers an investigation made in a wind tunnel to study the characteristics of submerged inlets at subsonic and transonic speeds.

The inlets were placed in one wall of the wind-tunnel test section. Because facilities for testing at transonic speeds are limited and the testing techniques are difficult, the present means of simulating duct entrances has been used as an expedient to obtain qualitive results. A comparison is made between two forms of the same basic submerged-type intake. These two inlets, one simulating an intake with parallel ramp walls and the other an intake with divergent ramp walls (an NACA submerged inlet), are compared on the basis of pressure recovery. This study should give a better understanding of the operation of submerged inlets in the transonic speed range and serve as a useful guide to the designer.

Some design considerations for extending the useful operating range of submerged inlets at transonic speeds are discussed.

## SYMBOLS

The symbols used are defined as follows:

| | |
|---|---|
| $A$ | duct-entrance area, square feet |
| $H$ | total pressure, pounds per square foot |
| $M$ | Mach number |
| $p$ | static pressure, pounds per square foot |
| $V$ | velocity, feet per second |
| $\rho$ | air density, slugs per cubic foot |
| $\frac{m_1}{m_o}$ | mass-flow ratio $\left(\frac{\rho_1 A_1 V_1}{\rho_o A_1 V_o}\right)$ |
| $\frac{H-p_o}{H_o-p_o}$ | ram-recovery ratio |
| $\frac{p}{H_o}$ | pressure ratio |
| $\frac{H}{H_o}$ | total pressure ratio |

The following subscripts are used in conjunction with some of the above symbols:

| | |
|---|---|
| $o$ | free stream |

[redacted]

1 conditions 1 inch behind duct entrance

2 conditions 5 inches behind duct entrance

## APPARATUS

### Wind Tunnel

The investigation was conducted in a small transonic wind tunnel. The tunnel has a closed throat and is of the nonreturn type (fig. 1). The 2.1- by 7.4-inch test section has a diverging ceiling and floor (2.1-inch dimension) with a total expansion angle of 1.0° in the vertical plane to compensate partially for boundary-layer growth. Air enters a settling chamber, flows through the wind tunnel, and finally exhausts from the tunnel diffuser at approximately atmospheric pressure. The air is pumped to the settling chamber by an aircraft centrifugal compressor driven by a variable-speed electric motor, rated 300 horsepower at 18,000 rpm. Control of the settling-chamber pressure, and thus of the tunnel velocity, was accomplished by varying the speed of the electric motor.

### Models and Auxiliary Equipment

The installations of the two inlets in the top wall of the test section are shown in figures 2(a) and 2(b). Pertinent intake dimensions are presented in figure 3 and provide the optimum design ascertained from previous tests (reference 1). The inlet entrances extended from wall to wall across the 2.1-inch dimension of the test section, and had a width-to-depth ratio of 4.2. Both of the inlets tested, one with parallel and the other with NACA divergent ramp walls, had 7° ramp angles. Air entering the submerged inlet at the lip (fig. 1) was diffused in the internal ducting, then passed through an ASME orifice meter, and was finally exhausted through a small centrifugal blower. The quantity of flow was measured by the orifice meter and was controlled by a throttle. The amount of air flow through the inlet, although augmented slightly by the blower, was limited by the pressure-recovery characteristics of the duct system. Thus, the inlet with the higher pressure recovery at a given Mach number was tested over the greater range of mass-flow ratios.

### Instrumentation

Pressure recoveries for both submerged inlets were measured with a 7-tube total-pressure rake installed in the duct 5 inches back of the lip leading edge. The rake was mounted normal to the duct width and passed through the center of the duct (fig. 3). The duct height at the

measurement station was 0.70 inch. Because the duct height at the entrance was 0.50 inch, internal diffusion losses due to an area increase of 40 percent are included in the measurements. The pressure losses were measured only at the center section; consequently, for the simulated NACA submerged inlet the losses due to turbulent mixing, as explained in reference 4, are not included. However, the measurements in this center plane should qualitatively indicate the inlet characteristics at high subsonic and transonic Mach numbers.

Static-pressure distributions down the center line of the ramp leading to the entrances were measured with flush orifices connected to a multiple-tube manometer. Measurements for computing wind-tunnel Mach number distributions were also obtained from flush static orifices distributed over a steel plate mounted on one side of the test section. Visual flow studies were made with a schlieren apparatus and with a shadowgraph apparatus utilizing a Libessart spark.

For this report, the free-stream Mach number is defined as the Mach number measured on the center of the tunnel floor one-quarter inch forward of ramp station 0. This location on the wind-tunnel floor was selected so that the inlet would have the least effect on the free-stream Mach number measurement. A direct-reading nomographic Mach meter, explained in reference 5, was used to indicate the wind-tunnel speed in terms of free-stream Mach number.

## TEST METHODS

Both inlets were tested from 0.20 Mach number to the maximum that could be obtained with this wind tunnel. The Mach number limit was 0.94 with the parallel-walled inlet, and 0.96 with the divergent-walled inlet. The maximum Mach number attainable with the parallel-walled inlet installed in the wind tunnel was determined by power limitations of the wind-tunnel motor-compressor unit; whereas with the divergent-walled inlet the limiting factor appeared to be the establishment of sonic velocity across the wind tunnel back of ramp station 0.

The range of mass-flow ratios varied with Mach number and inlet configuration. The following table indicates the mass-flow ratios that were obtainable during these tests:

| Mach number $M_o$ | Range of mass-flow ratio, $m_1/m_o$ | |
|---|---|---|
| | Parallel walls | Divergent walls |
| 0.20 | 0 to 1.2 | 0 to 1.2 |
| .40 | 0 to 1.2 | 0 to 1.2 |
| .60 | 0 to 0.8 | 0 to 1.0 |
| .80 | 0 to 0.8 | 0 to 0.8 |
| .90 | 0 to 0.2 | 0.4 to 0.8 |
| .94 | 0.6 | 0.4 to 0.8 |
| .96 | - - - | 0.4 to 0.8 |

## RESULTS

The Mach number distribution in the wind-tunnel test section, calculated from static pressures measured on one test-section wall, is shown in figure 4 for free-stream Mach numbers of 0.80 and 0.94 (as defined herein). The Mach number distributions are shown in this figure for the tunnel without inlets and with the parallel-walled inlet installed.

The effects of Mach number on the pressure recovery for both the parallel- and divergent-walled inlets are given in terms of ram-recovery ratio in figure 5, and in terms of total-pressure ratio in figure 6. The variations of ram-recovery ratio across the duct depth at the measurement station (fig. 3) for both inlets are presented in figure 7. These ram-recovery-ratio profiles were obtained for a mass-flow ratio of 0.6 at Mach numbers just above and just below that at which the pressure recovery decreased abruptly.

The pressure distributions along the ramp center line of each inlet for several free-stream Mach numbers are presented in figure 8, and the corresponding Mach number distributions are given in figure 9. The Mach numbers were computed by assuming isentropic flow, and thus are only approximations.

Shadowgraphs of the flow about the parallel-walled inlet for various Mach numbers and mass-flow ratios are shown in figure 10. Similar shadowgraphs for the divergent-walled inlet are presented in figure 11.

## DISCUSSION

### Wind-Tunnel Air-Flow Characteristics

For free-stream Mach numbers up to 0.90, the variation of Mach number along the wind-tunnel test section without the models installed was about 1 percent. However, the deviation became greater as the Mach number was increased beyond 0.90. The air flow in the tunnel finally choked at a free-stream Mach number, as measured at the start of the test section, of 0.94. (See fig. 4(b).) This limitation in maximum free-stream Mach number for the tunnel without inlets installed is probably due to insufficient compensation for the displacement of the air stream by the boundary layer of the test section.

In reviewing the results of this investigation, certain additional limitations of the experimental arrangement must be considered. The air flow about the inlet was constrained by the wind-tunnel walls. Also, the ratio of the inlet area of the duct to the cross-sectional area of the wind tunnel was relatively large (1 to 15). Consequently, the Mach number distribution in the test section was affected by mass-flow ratio (fig. 4(a)). However, the data presented should be useful qualitatively.

Shadowgraphs with either inlet installed indicate that at Mach numbers up to 0.93 the oblique shock disturbance, originating at the beginning of the test-section expansion, was weak; consequently, the shock is believed to have had a negligible effect on the conditions downstream. (See fig. 10(g).)

## Comparison of Pressure Recovery

It should be remembered that the pressure recoveries presented in this report were obtained only in a line normal to the duct width and passing through the duct center line. The transverse variation of pressure recovery has not been determined.

A significant effect of Mach number on the pressure recovery of the parallel-walled inlet was evident at Mach numbers between 0.75 and 0.82. In this Mach number range, for mass-flow ratios of 0.40 and greater, the pressure recovery in terms of ram-recovery ratio decreased sharply with increasing Mach number. (See fig. 5(a).) Such a sharp decline did not occur with the divergent-walled inlet until a free-stream Mach number of 0.90 was exceeded. (See fig. 5(b).) Violent wind-tunnel vibrations at the higher Mach numbers prevented the taking of data for mass-flow ratios below 0.40.

The increase in magnitude of the pressure recovery at the center plane for the divergent-walled inlet over that obtained with the parallel-walled inlet, at the Mach numbers and mass-flow ratios of these tests, can be attributed to the difference in the factors governing the boundary-layer growth along the ramp. Measurements have shown that the boundary-layer flow with the divergent-walled inlet was three-dimensional; consequently, its growth was less rapid than for the two-dimensional flow which existed with the parallel-walled inlet (reference 6). However, for both inlets, the decrease in pressure recovery at the center section with a decrease of mass-flow ratio was due to a thickening of the ramp boundary layer. This thickening was, in turn, a consequence of increased adverse pressure gradients along the ramp. The pressure recoveries given in figures 5(a) and 5(b) are an indication of the relative boundary-layer thicknesses of the two types of inlets. Measurements of the velocity profile just behind the beginning of the parallel-walled ramp showed that the boundary layer was turbulent.

It should be noted in figure 5(a) that the curves showing ram-recovery ratio for the parallel-walled inlet are extrapolated. In the Mach number range between 0.79 and 0.94 the air flow in the duct was unstable and it was not possible to obtain consistent data in this range. However, the pressure recovery did decrease markedly, and it was impossible to obtain mass-flow ratios greater than 0.20 with the test equipment. For a Mach number of 0.94 the air flow became steady at a mass-flow ratio of 0.60.

Shadowgraph studies of the air flow with the parallel-walled inlet did not show the presence of strong shock waves for Mach numbers just before and after the sharp decline in pressure recovery ($M_o$ about 0.75 and 0.82, respectively). There was evidence, however, of a shock disturbance which extended only a short distance above the ramp surface at the beginning of the ramp and coincided with a thickening of the boundary layer along the ramp surface (figs. 10(b) and 10(d).) Figure 7(a) shows a decrease in pressure recovery for the parallel-walled inlet as the free-stream Mach number was increased from 0.76 to 0.80. At greater Mach numbers, visual observations of the multiple manometer registering the ram-pressure recovery indicated the unstable nature of the air flow in the duct system. Visual schlieren studies showed boundary-layer separation along the ramp for Mach numbers just greater than those at which the sharp decrease of pressure recovery occurred. A return to a more stable type of boundary-layer air flow is indicated by the shadowgraph for a free-stream Mach number of 0.94 (fig. 10(h)).

The pressure-recovery characteristics of the divergent-walled inlet together with shadowgraphs of the air flow (figs. 5(b) and 11, respectively) indicate that the interaction of the shock wave with the thinner boundary layer on the ramp of the divergent-walled inlet (reference 6) was much less severe than the interaction of the shock wave with the thicker boundary layer on the parallel-walled ramp. First evidence of a local shock-wave disturbance with the divergent-walled inlet occurred at approximately 0.82 Mach number. However, the abrupt decrease in pressure recovery was delayed to a free-stream Mach number of approximately 0.94.

For Mach numbers of 0.94 and greater, the shadowgraphs of the flow with the divergent-walled inlet (fig. 11) show shock waves originating at two locations along the ramp, a series of oblique waves at the start of the ramp, and a normal shock at about 70 percent of the ramp length. However, the air flow with the divergent-walled inlet, and thus presumably the shock-wave pattern, is three-dimensional. From figure 11 it appears that the normal shock wave extended between the upper edges of the ramp side walls. As the Mach number was increased from 0.94, this normal shock wave moved downstream. At the free-stream Mach number of 0.96 and mass-flow ratios of 0.6 and 0.8, the strength of the normal shock wave possibly became great enough to cause separation of the ramp boundary layer and a consequent drop in ram-pressure recovery. The tendency toward separation with increasing Mach number is shown by the ram-recovery-ratio profiles in figure 7(b) for the Mach numbers from 0.90 to 0.955.

## Design Considerations

It would seem probable that the transonic Mach number range for satisfactory operation of NACA submerged inlets could be extended. Of the several methods of accomplishing improved inlet performance, the first is concerned with consideration of the flow field into which the inlet is placed.

At moderate supersonic speeds, the local air flow over portions of certain body shapes can be at a lower Mach number than the free stream. For a conical body, reference 7 has shown that, depending on the cone angle, subsonic flow can exist on the surface of a cone even though the free-stream Mach number exceeds 1.0. Therefore, it would seem that the shape of the fuselage and the location of the inlet on the fuselage might be selected so that the effect of the reduced Mach number at the fuselage surface could be used advantageously to extend the transonic operation of submerged inlets.

Modification of the inlet itself might also prove beneficial, and a second method of extension might be the positioning of the normal shock wave forward along the ramp. The shock wave would then occur over a smaller percentage of the inlet width, and the amount of air with reduced pressure taken into the duct would be correspondingly less. Since the ramp boundary layer is thinner at the forward position, the interaction between this boundary layer and the shock wave would be less severe.

Boundary-layer control by slots or porous suction might also minimize the boundary-layer-shock-wave interaction.

## CONCLUDING REMARKS

A qualitative comparison of two types of submerged inlets at subsonic and transonic Mach numbers has shown that the pressure recovery for the parallel-walled inlet decreased abruptly at Mach numbers between 0.75 and 0.82, depending on the mass-flow ratio. The corresponding Mach number range for the divergent-walled inlet was 0.90 to 0.94.

The increase in Mach number for satisfactory pressure recovery with the divergent-walled inlet is attributed to a less severe interaction between the shock waves and the ramp boundary layer. The thinner boundary layer of the three-dimensional flow on the divergent-walled inlet apparently has less tendency to separate under adverse pressure gradients than has the thicker boundary layer in the two-dimensional flow of a parallel-walled inlet.

Ames Aeronautical Laboratory,
National Advisory Committee for Aeronautics,
Moffett Field, Calif.

[redacted]

REFERENCES

1. Mossman, Emmet A., and Randall, Lauros M.: An Experimental Investigation of the Design Variables for NACA Submerged Duct Entrances. NACA RM A7I30, 1948.

2. Martin, Norman J., and Holzhauser, Curt A.: An Experimental Investigation at Large Scale of Several Configurations of an NACA Submerged Air Intake. NACA RM A8F21, 1948.

3. Hall, Charles F., and Barclay, F. Dorn: An Experimental Investigation of NACA Submerged Inlets at High Subsonic Speeds. I – Inlets Forward of the Wing Leading Edge. NACA RM A8B16, 1948.

4. Delany, Noel K.: An Investigation of Submerged Air Inlets on a 1/4-Scale Model of a Typical Fighter-Type Airplane. NACA RM A8A20, 1948.

5. Liepmann, Hans Wolfgang: The Interaction between Boundary Layer and Shock Waves in Transonic Flow. Jour. Aero. Sci., vol. 13, no. 12, Dec. 1946.

6. Dryden, Hugh L.: The Aeronautical Research Scene – Goals, Methods, and Accomplishments. The 1949 (37th) Wilbur Wright Memorial Lecture, London, Apr. 28, 1949. Royal Aeronautical Society.

7. Taylor, G. I., and Maccoll, J. W.: The Air Pressure on a Cone Moving at High Speeds. I and II Proceedings of the Royal Society (London), Ser. A., vol. 139, no. 838, Feb. 1, 1933.


Figure 1.– General view of the 2.1– by 7.4–inch wind tunnel.

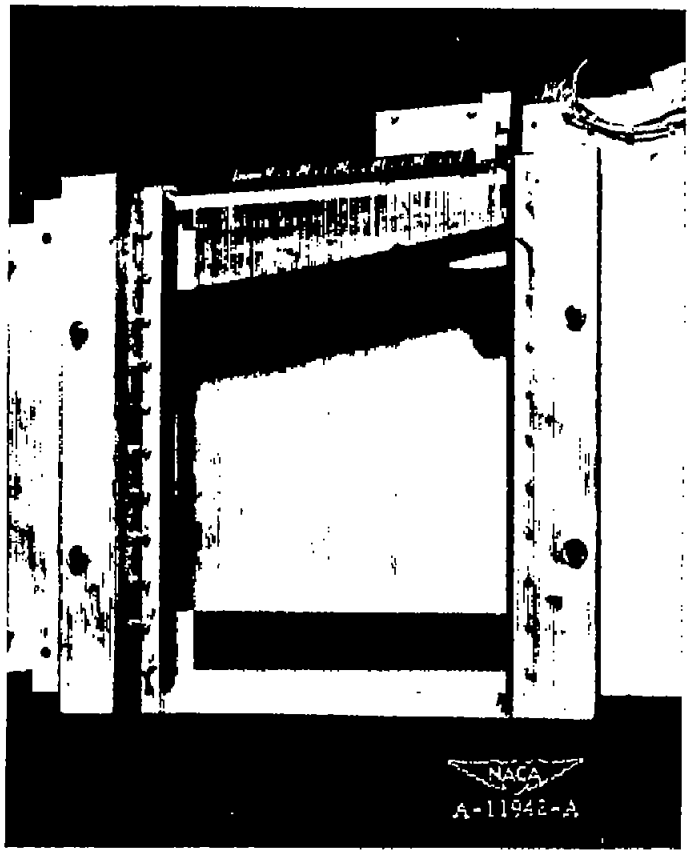


(a) Parallel-walled inlet.


(b) Divergent-walled inlet.

Figure 2.- Wind-tunnel test section with inlets installed.

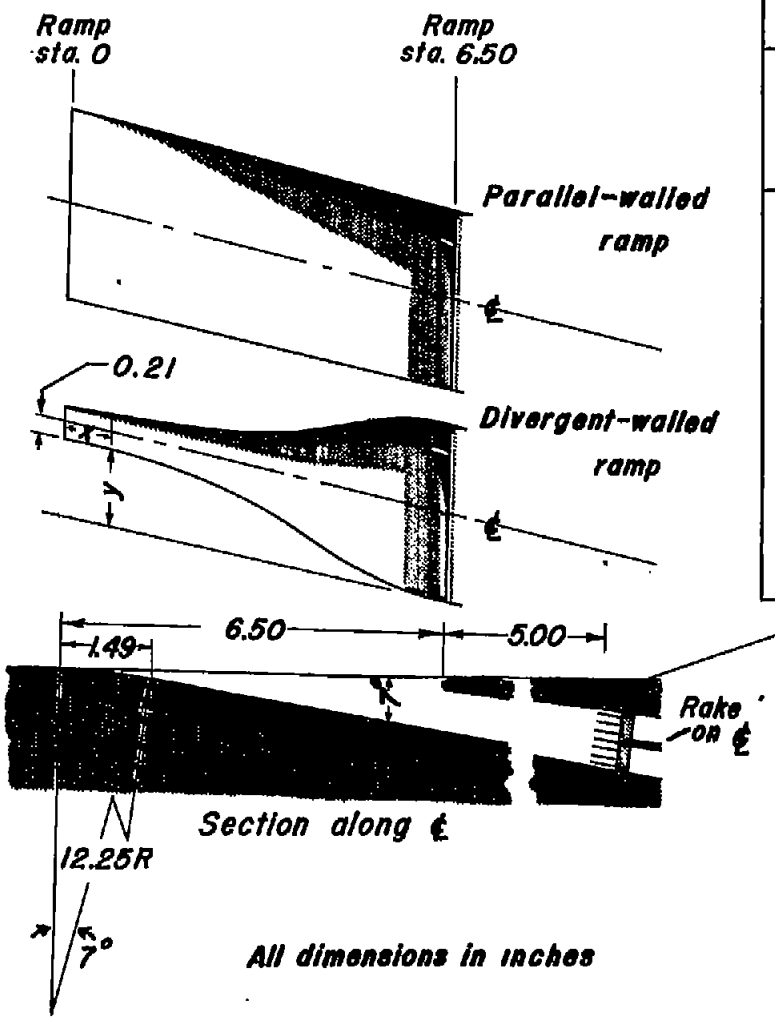


| Lip coordinates | | | | | |
|---|---|---|---|---|---|
| Lip sta. x—(in) | Ordinate y—(in) | | Lip sta. x—(in) | Ordinate y—(in) | |
| | Outside | Inside | | Outside | Inside |
| 0 | .182 | .182 | 0.75 | .063 | .358 |
| 0.05 | .130 | .237 | 1.00 | .065 | .385 |
| 0.10 | .114 | .258 | 1.50 | .079 | .439 |
| 0.15 | .102 | .273 | 2.00 | .104 | .504 |
| 0.20 | .092 | .284 | 2.50 | .128 | .578 |
| 0.30 | .078 | .300 | 3.50 | .177 | .717 |
| 0.40 | .070 | .314 | 4.50 | .226 | .856 |
| 0.50 | .065 | .326 | 5.50 | .274 | .994 |
| 0.60 | .062 | .340 | | | |

| Divergent—wall coordinates | | | |
|---|---|---|---|
| Ramp sta. x—(in) | Ordinate y—(in) | Ramp sta. x—(in) | Ordinate y—(in) |
| 0 | .840 | 3.62 | .565 |
| 0.74 | .840 | 4.20 | .408 |
| 1.32 | .830 | 4.77 | .250 |
| 1.90 | .809 | 5.34 | .091 |
| 2.47 | .726 | 5.76 | .006 |
| 3.05 | .645 | 6.50 | 0 |

Figure 3.— General arrangement and dimensions of the submerged-type inlets.

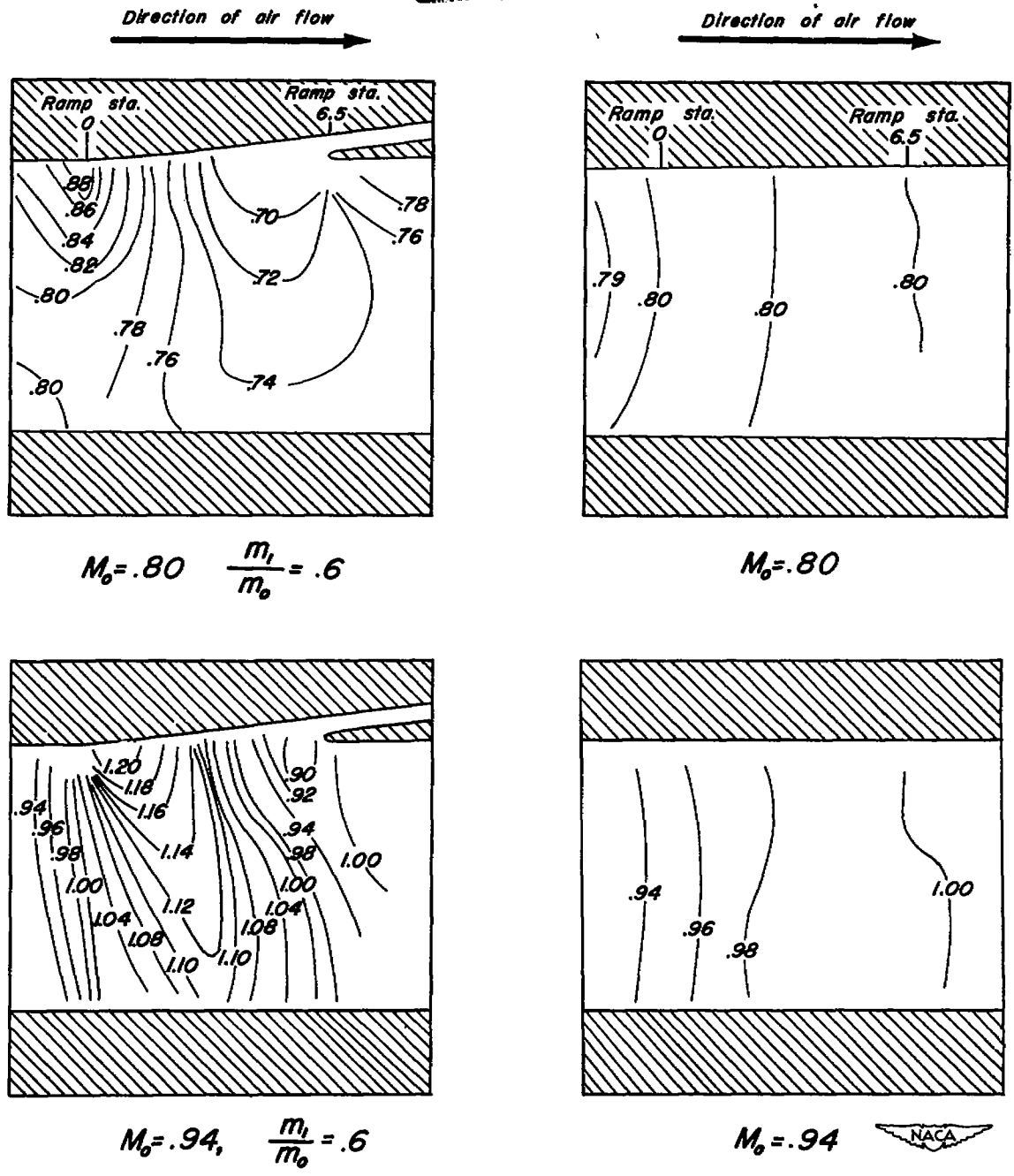


(a) Tunnel with parallel-walled inlet.

(b) Tunnel without inlets installed.

Figure 4.- Mach number distributions in the wind-tunnel test section.

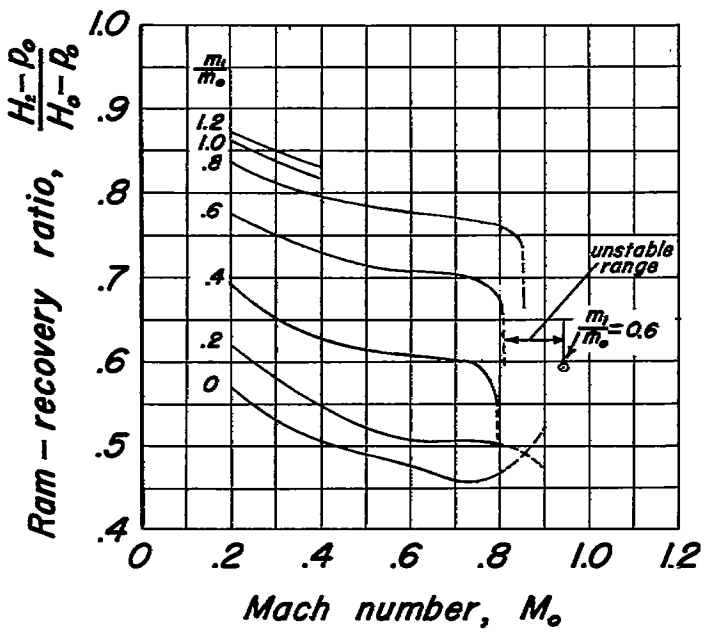


(a) Parallel-walled inlet.

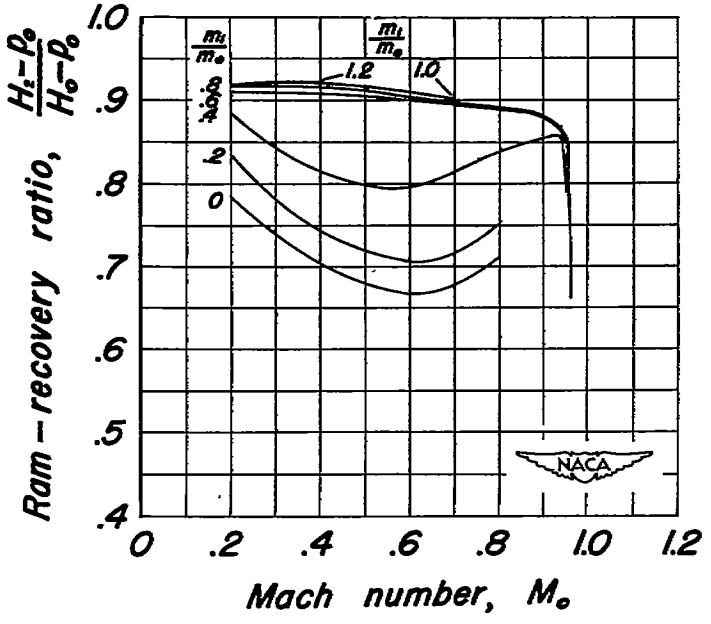


(b) Divergent-walled inlet.

Figure 5.- Variation of ram-recovery ratio with free-stream Mach number for various mass-flow ratios.

[redacted]

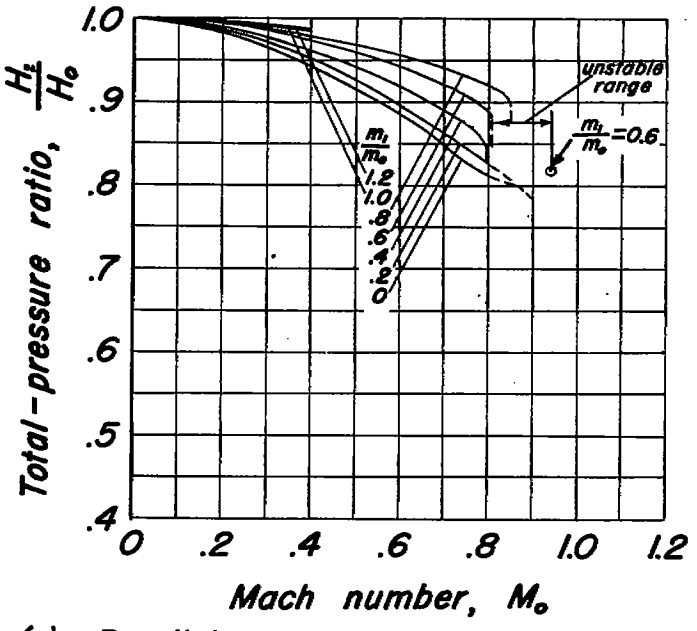


(a) Parallel—walled inlet.

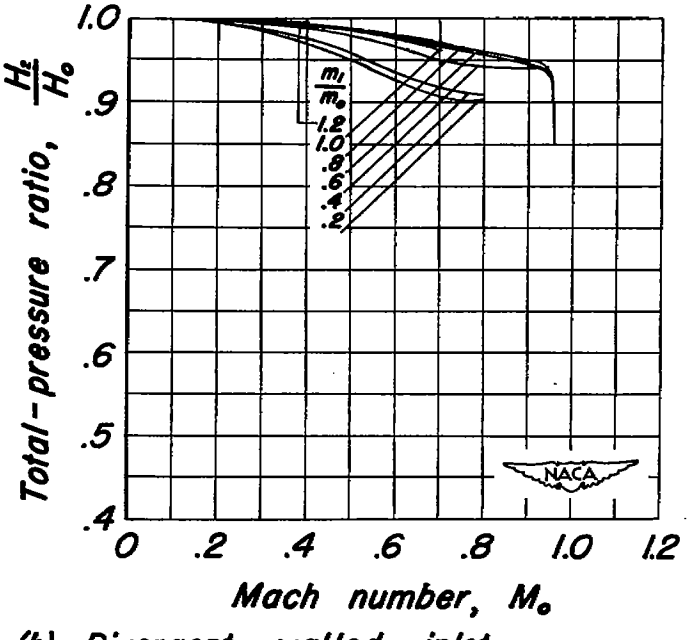


(b) Divergent—walled inlet.

Figure 6.- Variation of total-pressure ratio with free-stream Mach number for various mass-flow ratios.

[redacted]

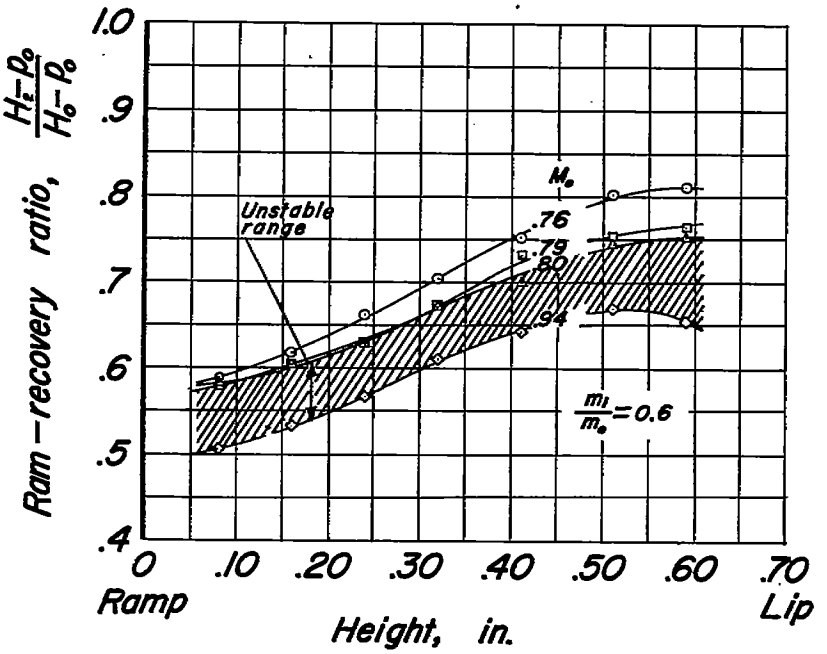


(a) Parallel-walled inlet.

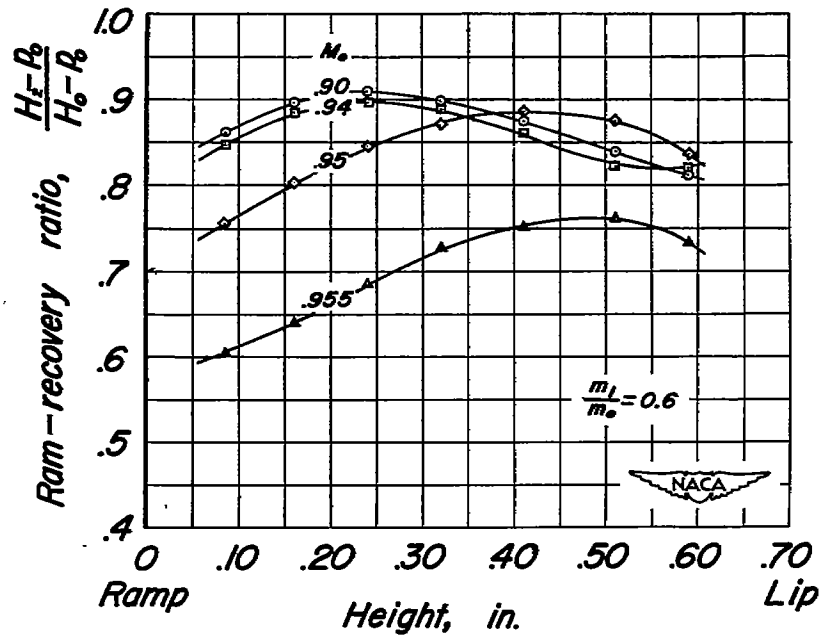


(b) Divergent-walled inlet.

Figure 7.- Ram-recovery profiles in the duct, 5 inches back of the lip leading edge.

[redacted]

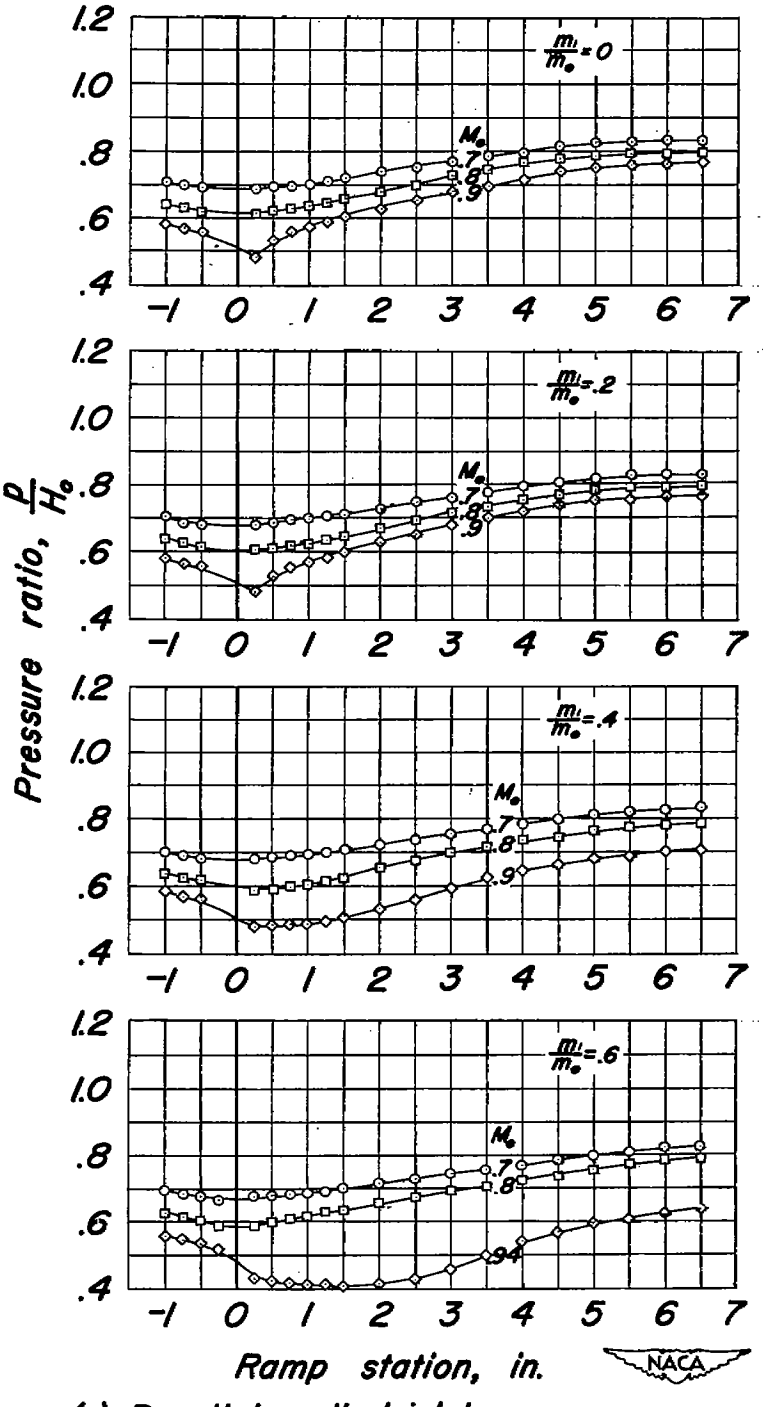


(a) Parallel-walled inlet.

*Figure 8.– Pressure distribution along the ramp center line for various free-stream Mach numbers.*

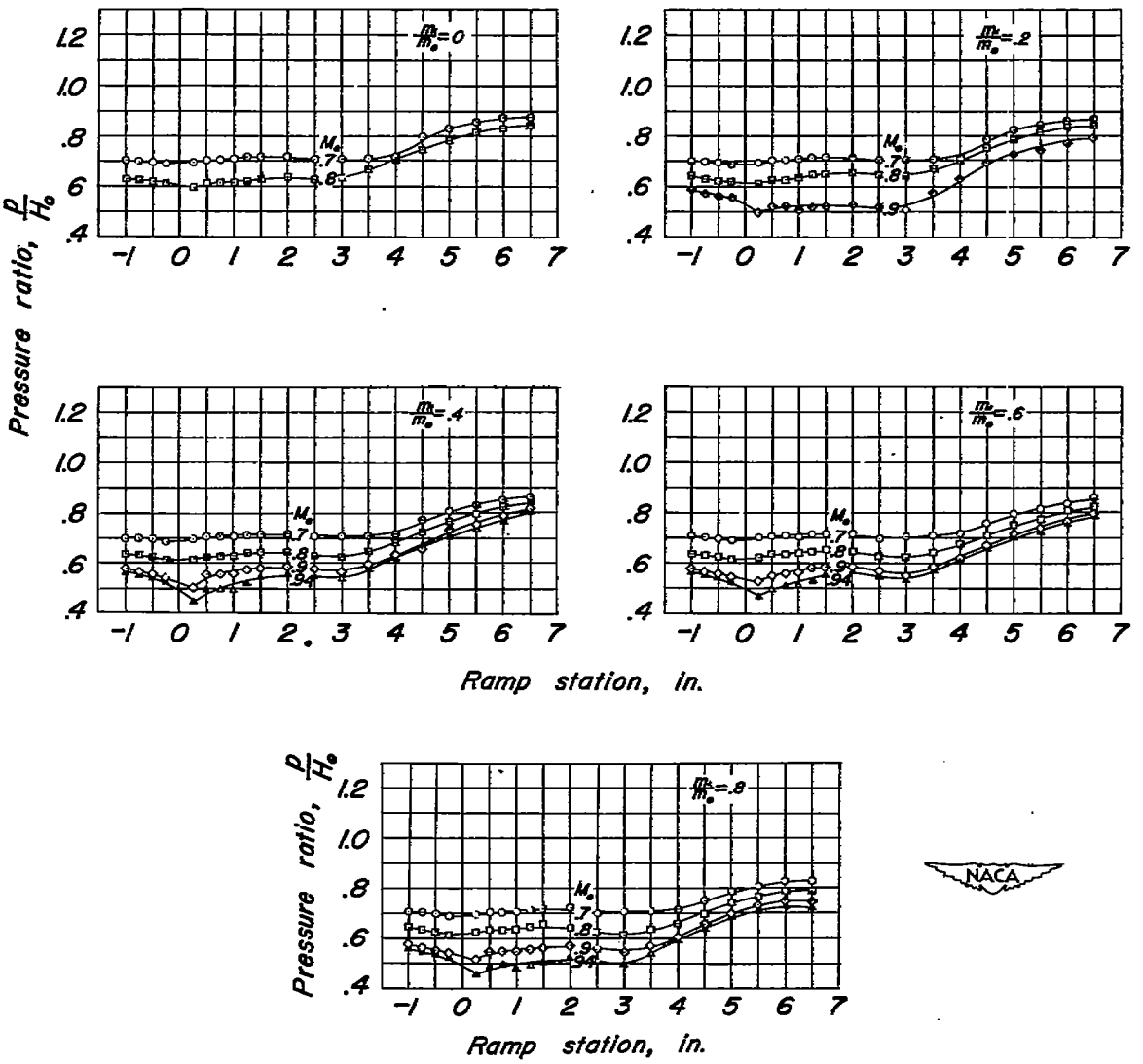


*(b) Divergent-walled inlet.*

*Figure 8.- Concluded.*

[redacted]

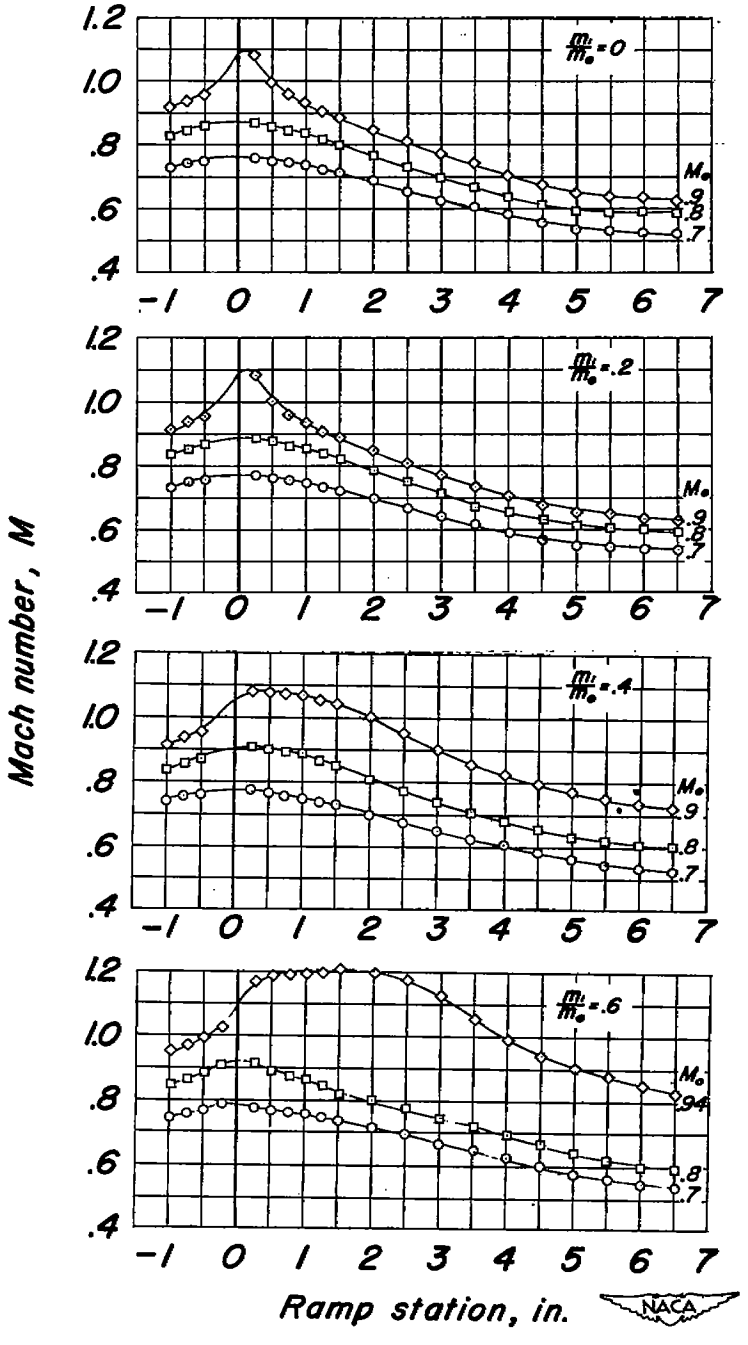


(a) Parallel-walled inlet

*Figure 9.- Mach number distribution along the ramp center line for various free-stream Mach numbers.*

[redacted]

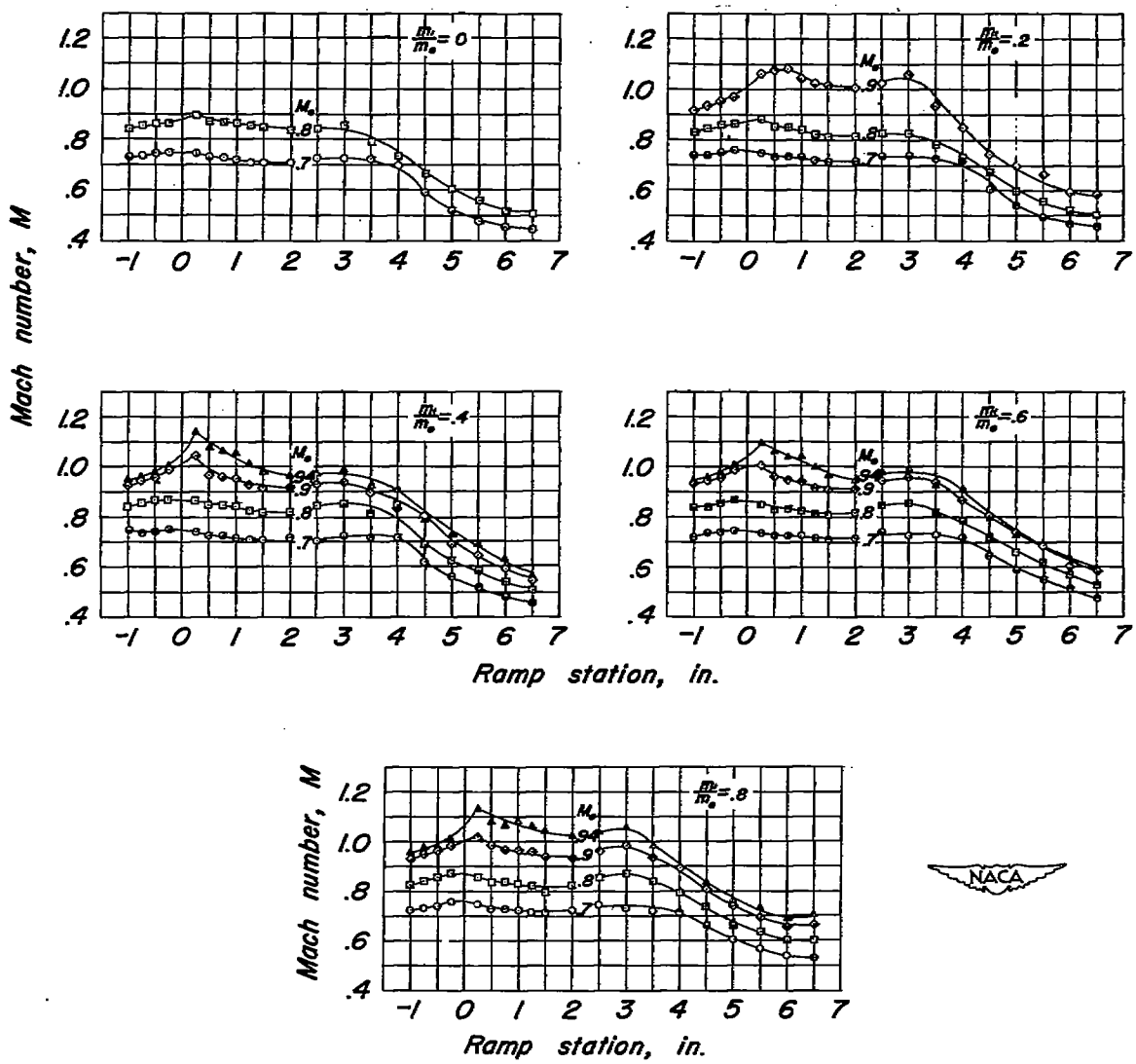


(b) Divergent-walled inlet.

Figure 9.- Concluded.

(a) $M_o = 0.75$; $\frac{m_1}{m_o} = 0.8$.

(b) $M_o = 0.80$; $\frac{m_1}{m_o} = 0.6$.

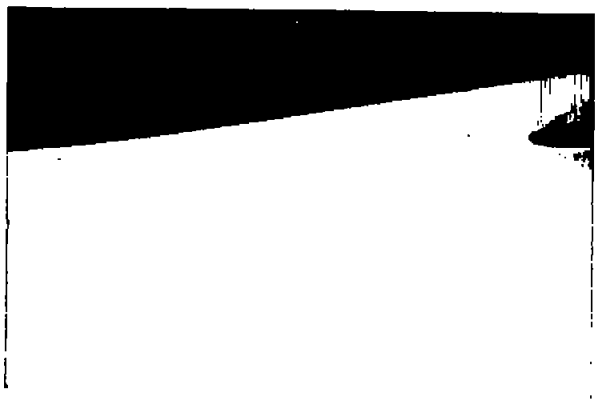

(c) $M_o = 0.82$; $\frac{m_1}{m_o} = 0.2$.

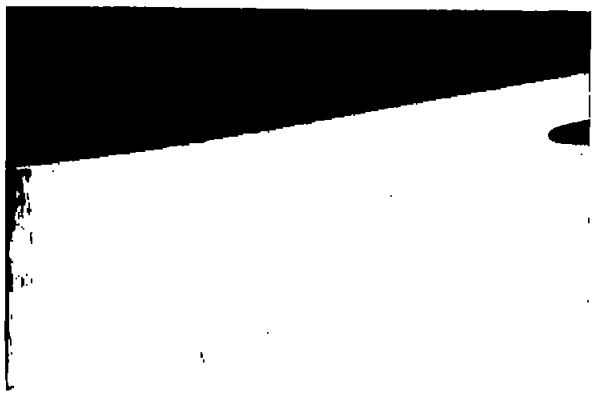

(d) $M_o = 0.82$; $\frac{m_1}{m_o} = 0.6$.

NACA
A-14019

Figure 10.— Shadowgraphs of the air flow along the ramp of the parallel-walled inlet.

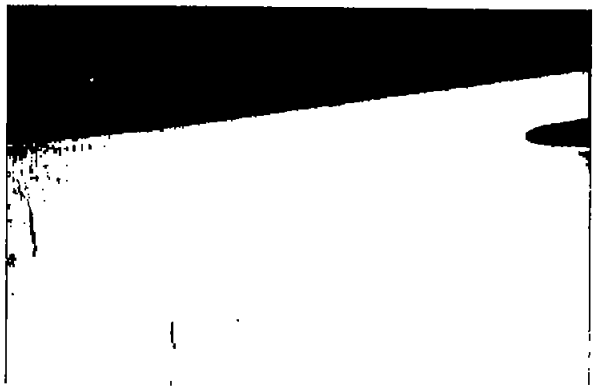

(e) $M_o = 0.88$; $\frac{m_1}{m_o} = 0.2$.

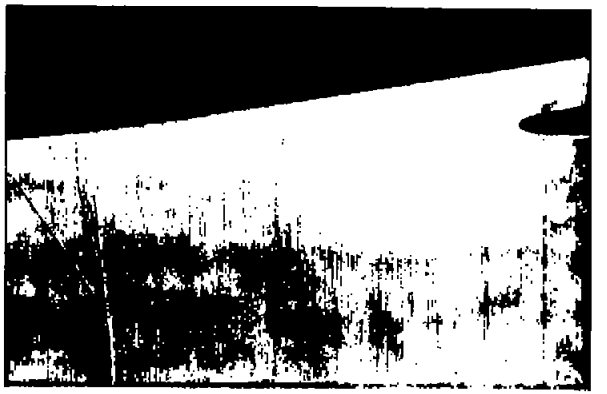

(f) $M_o = 0.90$; $\frac{m_1}{m_o} = 0.2$.

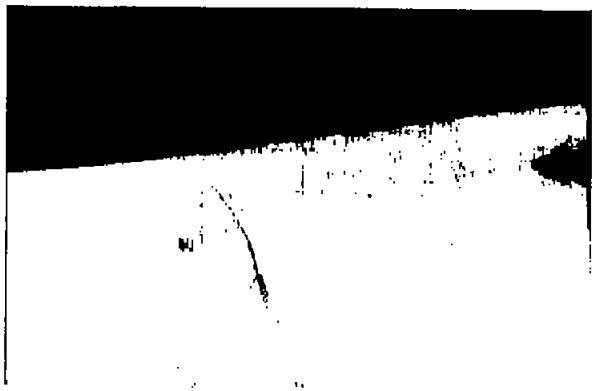

(g) $M_o = 0.93$; $\frac{m_1}{m_o}$ (unsteady).

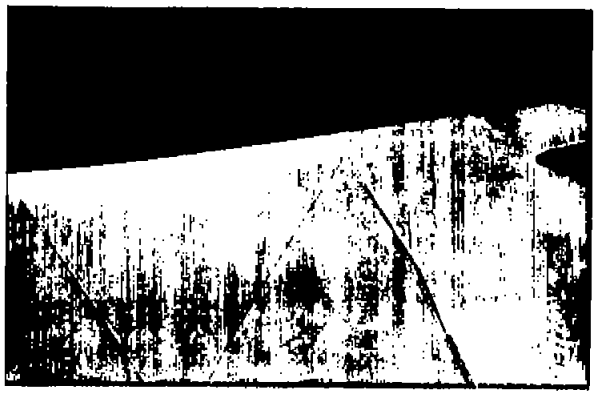

(h) $M_o = 0.94$; $\frac{m_1}{m_o} = 0.6$.

NACA
A-14018

Figure 10.– Concluded.

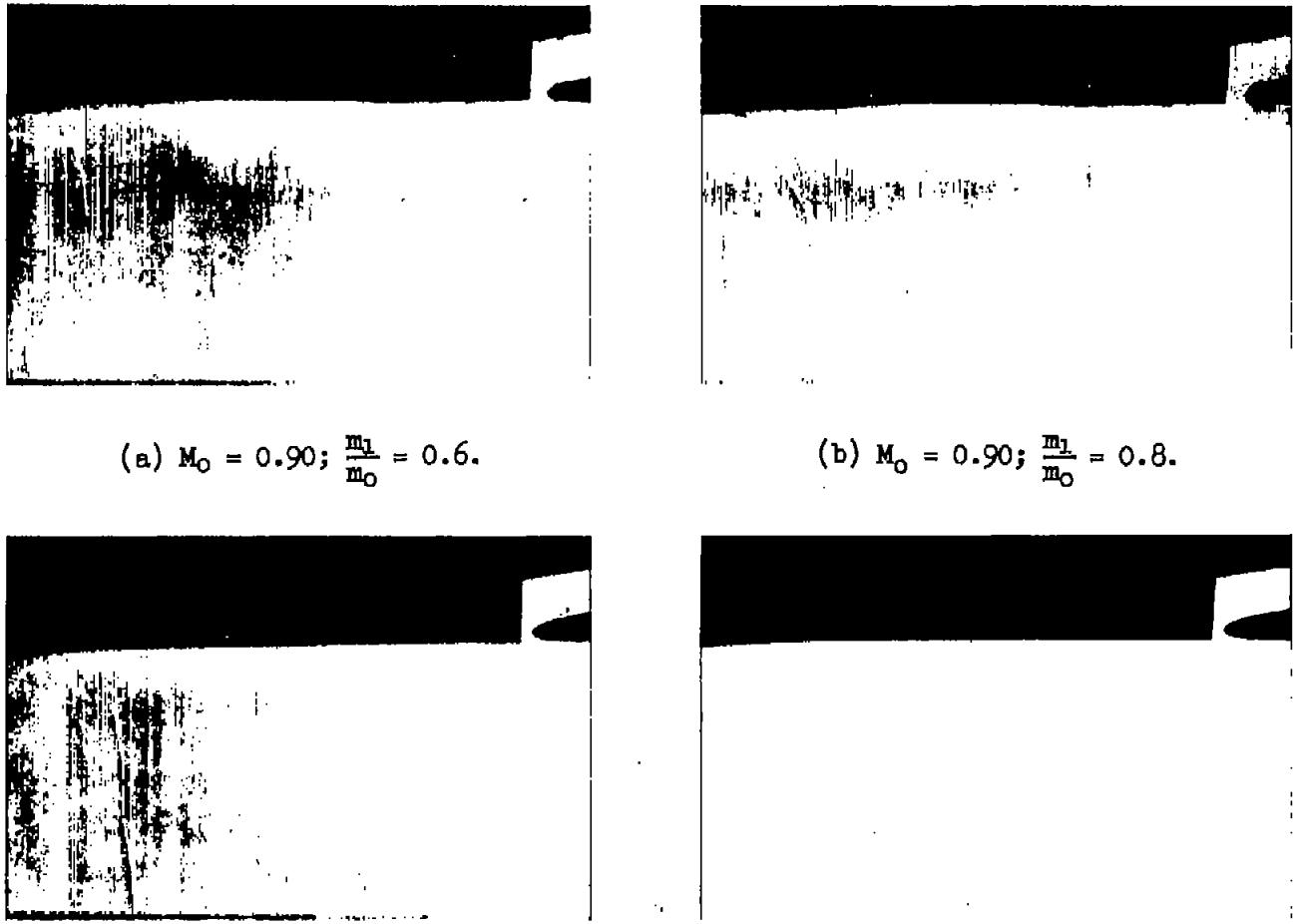

(a) $M_o = 0.90$; $\frac{m_1}{m_o} = 0.6$.

(b) $M_o = 0.90$; $\frac{m_1}{m_o} = 0.8$.

(c) $M_o = 0.92$; $\frac{m_1}{m_o} = 0.8$.

(d) $M_o = 0.95$; $\frac{m_1}{m_o} = 0.8$.

NACA
A-14020

Figure 11.- Shadowgraphs of the air flow along the ramp of the divergent-walled inlet.

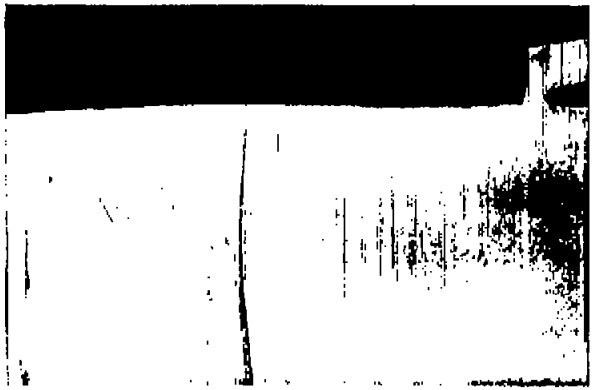

(e) $M_o = 0.94$; $\frac{m_1}{m_o} = 0.6$.

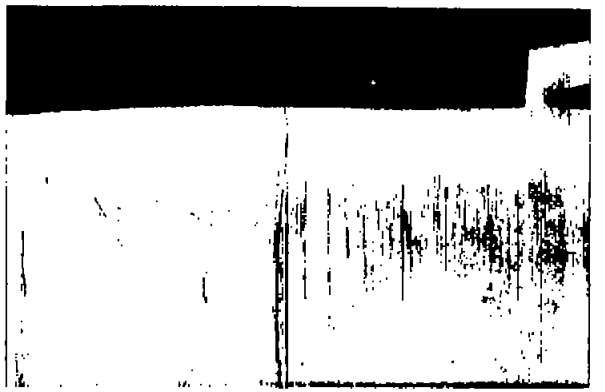

(f) $M_o = 0.94$; $\frac{m_1}{m_o} = 0.8$.

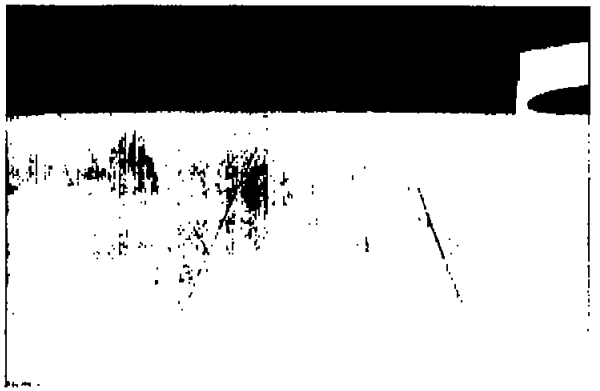

(g) $M_o = 0.96$; $\frac{m_1}{m_o} = 0.6$.

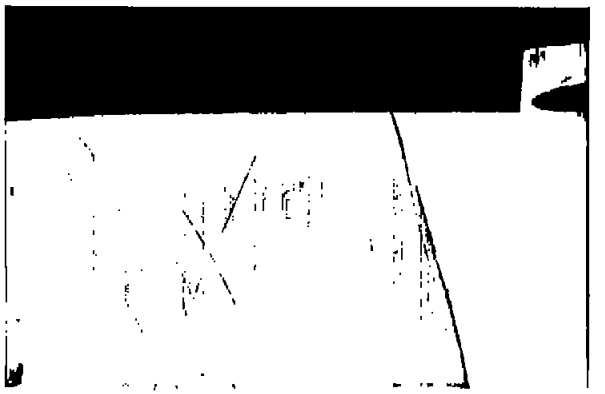

(h) $M_o = 0.96$; $\frac{m_1}{m_o} = 0.8$.

NACA
A-14021

Figure 11.– Concluded.